Bulletin of the Seismological Society of America, Vol. 103, No. 5, pp. 2670–2679, October 2013, doi: 10.1785/0120120335

Energy Flux of Propagating Ruptures with Cohesive Force

by Andrea Bizzarri

Abstract The energy flux F at the rupture tip has been previously computed only for 2D steady-state singular cracks. In this paper, I compute F for fully dynamic 3D ruptures, propagating both with constant and variable rupture speed (v_r) over finite faults directed by a governing law with a cohesive zone (and thus nonsingular ruptures). The results presented here indicate that F is positive and increasing over the whole range of v_r from zero up to P-wave speed. This is in contrast with 2D steady-state singular cracks, which predict the existence of a forbidden zone in the range of rupture speeds because in that interval F would be negative. Moreover, I found that in 3D ruptures with cohesive force, F is proportional to v_r, again in contrast to 2D steady-state singular cracks, in which F is not a unique function of v_r and also exhibits an inverse dependence on v_r. More specifically, it emerges that fast earthquakes tend to have a higher energy flux at the crack tip compared with slow ruptures. Finally, I show that the magnitude of F is basically due to its component aligned in the direction of the initial shear stress.

Introduction

The crack growth process involves material separation, which is an energy-consuming physical process. As a consequence, a positive energy flux is required at the tip of a rupture. More explicitly, the leading edge of the crack, which is responsible for the decohesion mechanism, requires some energy to be supplied from the outer field to the crack edge region (Broberg, 1989). On the other hand, the eventual trailing edge of the crack, which consists of some healing mechanism, does not require the energy supply; therefore, there are no theoretical limitations for the rupture speed of that front. As pointed out by Winkler *et al.* (1970) and Curran *et al.* (1970), the leading-edge propagation can be possible at any speed only in cases where the energy is supplied directly to the crack without recourse to the elastic stress waves (see also Samudrala *et al.*, 2002). Broberg (1989) concludes that a singular mode I or II leading edge cannot propagate at constant, or smoothly varying, velocity in the interval $[v_R, v_S]$ (v_R being the Rayleigh speed and v_S being the S-wave speed), because the energy flow to the edge is positive only for sub-Rayleigh speeds (for modes I and II) and for supershear speeds (for mode II). As discussed by Broberg (1989), the requirement of a positive energy flux is inescapable for the leading edge; the only possibility for a crack propagating at fixed speed is to alternate sub-Rayleigh and supersonic speeds, so that, on average, the forbidden region is penetrated. As summarized by Broberg (1999; fig. 9.3.1), in the range of v_r between v_R and v_S, a mode II singular crack would become an energy source (i.e., energy releasing) instead of an energy sink (i.e., energy absorbing; see also Freund, 1979; Broberg, 1989). Indeed, from that figure we can see that as the rupture speed assumed in a 2D steady-state singular crack (having an abrupt stress drop) approaches the boundaries of the forbidden zone, the energy flux decreases and tends to become negative. (Incidentally, we note that the same occurs when v_r approaches v_P, which is the maximum allowable speed for pure mode II problems.)

A fundamental result recently found by Bizzarri and Das (2012) is that for 3D nonsingular ruptures (for which the stress release is accomplished in a process zone of finite length), where there is a complex mixture of shear modes II and III of fracture (and with possible rake rotation), the energy flux is positive for mode II over the whole range of rupture speeds, from 0 to v_P. This is intimately related to the fact that in 3D, even in the idealized case of linear slip-weakening (SW) friction law (Ida, 1972), there is no so-called forbidden zone $v_R \le v_r \le v_S$ (Bizzarri and Das, 2012).

In general, the fracture energy density $E_G([E_G] = \mathrm{J/m^2})$ in each fault point ξ is defined as (e.g., Bizzarri, 2010; see also equation 5.3.19 of Freund, 1990):

$$E_G(\xi,t) = \int_0^{+\infty} [\mathbf{T}(\xi,t) - \mathbf{T}_{\mathrm{res}}(\xi)] \cdot \mathbf{v}(\xi,t)\mathrm{d}t = \int_0^{+\infty} [\tau(\xi,t) - \tau_{\mathrm{res}}(\xi)] u(\xi,t)\mathrm{d}u, \qquad (1)$$

in which $\mathbf{T}$ and $\mathbf{T}_{\mathrm{res}}$ are the fault shear traction vector and its residual level, respectively; τ and τ_{res} are their Euclidean norms; and the last equality holds when the traction is collinear to the fault slip velocity. E_G, which physically represents the amount of energy required to create a new unit area of fractured surface, is often denoted with the symbol γ_F

(e.g., Achenbach, 1972; his equation 2.6, among many others) or with the symbol γ (e.g., Ida, 1972). In the special case of the linear SW model with homogeneous properties, since $\tau_{res} = \tau_f$ (so that the integrands are not null only up to $t = T_b$, the breakdown time, or analogously only up to $u = d_0$, respectively), we simply have

$$E_G = \Delta\tau_b \frac{d_0}{2}, \tag{2}$$

which depends only on the constitutive parameters (d_0 is the characteristic SW distance and $\Delta\tau_b \underset{\text{df}}{=} \tau_u - \tau_f$ is the breakdown stress drop, τ_u being the upper yield stress, and τ_f being the residual level after the stress release). In homogeneous conditions, equation (2) implies that no predictions can be made on the basis of the energetic arguments discussed thus far regarding the allowed values of the rupture speeds (this conclusion also holds in the pure mode II case) and similarly implies that—for linear SW law with homogeneous properties—E_G should be a material property. On the other hand, in the case of constitutive models different from the SW law it has been shown (Bizzarri, 2010) that for homogeneous subshear ruptures roughly $E_G \propto \sqrt{1 - \frac{v_r^2}{v_S^2}}$, but for supershear ruptures it is difficult to infer a clear dependence of fracture energy density on rupture speed, especially in heterogeneous configurations. With these more realistic friction laws it emerges that E_G is not an intrinsic material property (Bizzarri, 2010).

It is interesting to consider the rate at which the mechanical energy is extracted from a volume V by the fracture process. This quantity, denoted by F, is equal to the rate of the work due to the external forces minus the rate of increase of the total energy in V (see Achenbach, 1972; his equation 2.5). Within the framework of the Griffith's theory (Griffith, 1920), the energy extracted from the body containing the rupture is totally converted into the surface energy of the newly formed surfaces, so that I can write

$$F(t) = \dot{U}_G(t), \tag{3}$$

in which the overdot indicates the time derivative and U_G expresses the total fracture energy (e.g., Bizzarri, 2011; his equation 19) as

$$U_G(t) = \iint_{\Sigma(t)} E_G(\xi)\mathrm{d}\xi, \tag{4}$$

with $\Sigma(t)$ being the fractured (or broken) region at time t. The quantity F in (3) has the physical dimensions of energy per unit time ($[F] = W = \mathrm{J/s}$). It should be noted that the equality of energy flux out of a block of material of volume V (usually referred to as the difference between strain energy flux and radiated energy) to the rate of total fracture energy is exact only for quasistatic (the J integral; Cherepanov, 1967; Rice, 1968) or steady-state ruptures (Ida, 1972). For variable rupture speeds, or heterogeneous rheological properties, the energy flow will also include the strain energy flux to the fault tip, the radiated energy leaving the volume (which is a time-dependent term), and the noise due to stress variations (the so-called Kostrov's term; see Favreau and Archuleta, 2003, Rivera and Kanamori, 2005, Madariaga, 2012 for a discussion).

In the special case of a governing model that predicts a constant fracture energy density over the fault surface—as the linear SW law—equation (4) simply reads

$$F(t) = \dot{\Sigma}(t)E_G, \tag{5}$$

where $\dot{\Sigma}(t)$ expresses the rate of the variation of the fractured region. The computation of $F(t)$ from equation (5) is straightforward because, in dynamic models of faulting, the location of the rupture tip is known at all times. Notably, equation (5) can be further simplified in the case of a bilateral 2D, pure mode II rupture on the $x_2 = 0$ plane and moving along x_1; in this case $\dot{\Sigma}(t)$ becomes the rate of increase of the broken length along x_1, which in turn can be expressed as $2v_r(t)$. Equation (5) then becomes $f(t) = 2v_r(t)E_G$, in agreement with equation (6.40) of Achenbach (1972; see also Atkinson and Eshelby, 1968). (The lower case f emphasizes that in this particular case it is the rate of work per unit length along x_3 that is calculated, so that $[f] = \mathrm{W/m}$. The resulting F can be arranged as $F(t) = 2v_r(t)W^f E_G$, in which W^f is the width of the fault.)

In a general case of a spontaneous dynamic rupture (i.e., not stationary), the rate of work F is expressed as follows:

$$F(t) = \iint_{\Pi(t)} (\mathbf{T}(\xi, t) - \mathbf{T}_{\text{res}}(\xi)) \cdot \mathbf{v}(\xi, t)\mathrm{d}\xi, \tag{6}$$

which generalizes equation (2.18) of Achenbach (1972) pertaining to a 2D, plane, nonstationary, singular crack. In equation (6) $\Pi(t)$ denotes a zone surrounding the crack tip $\Gamma(t)$, which is defined as the locus of points exceeding, at time t, a threshold value of the slip velocity ($v_l = 0.01$ m/s). We have shown that this value is small enough to capture all the details of the rupture and the birth of the supershear front. In the special case of the SW law, the sliding logic also says that the slip begins only once τ_u is reached; we have also shown that the conditions to detect the rupture front from the slip velocity criterion (v_l) or from the traction value (τ_u) give identical results. It is apparent that the integrand of equation (6) is the same as that of equation (5) (once one has substituted the definition of E_G from equation 1); the link between these two equations is discussed in more detail in Appendix A.

In the case of a singular crack, $\Pi(t)$ is an arbitrarily small region containing $\Gamma(t)$; within the framework of a governing model with a cohesive zone, as the SW law, $\Pi(t)$ has to be interpreted as the process zone (formally, it represents the length of the cohesive zone at time t, $X_b(t)$).

Equation (6) is appropriate for propagating ruptures; indeed the domain of integration in equation (6) explicitly depends on time, as well as the integrand function. An alternative version of this equation (with opportune manipulations

to make it adequate for a 3D geometry) can be also found in Freund (1972; see also Freund, 1990) and it is reported by Achenbach (1972; his equation 2.28):

$$F(t) = \lim_{\Lambda\to 0} \iint_{\Lambda} (T_{ij}(\xi,t) n_j v_i(\xi,t) + \frac{1}{2} T_{ij}(\xi,t) u_i(\xi,t) v_n(\xi,t) + \frac{1}{2} \rho v_i(\xi,t) v_i(\xi,t) v_n(\xi,t)) \mathrm{d}\xi, \quad (7)$$

in which Λ is a loop (lying on the fault surface) surrounding the rupture tip and v_n is the component of the velocity of a point of the loop Λ in the direction of the outward normal. As pointed out by Achenbach (1972; see the discussion after his equation 2.28), the two formulations are equivalent.

The Numerical Model

In this paper, I consider a vertical strike-slip fault embedded in a perfectly elastic and isotropic medium. The geometry of the problem is reported in figure 2 of Bizzarri (2010) and the elastodynamic problem is solved numerically (Bizzarri and Cocco, 2005; Bizzarri, 2009). The initial rake angle is $\varphi_0 = 0$ and the residual stress is spatially homogeneous (i.e., $\|\mathbf{T}_{\mathrm{res}}(\xi)\| = \tau_f$), so that equation (6) simply reads

$$F(t) = \iint_{\Pi(t)} \left[\left(T_1(\xi,t) - \tau_f \frac{v_1(\xi,t)}{v(\xi,t)} \right) v_1(\xi,t) + \left(T_3(\xi,t) - \tau_f \frac{v_3(\xi,t)}{v(\xi,t)} \right) v_3(\xi,t) \right] \mathrm{d}\xi, \quad (8)$$

in which the subscripts 1 and 3 define the along-strike and along-depth components, respectively, of the vectors $\mathbf{T}$ and $\mathbf{v}$, and $v = \|\mathbf{v}\| = (v_1^2 + v_3^2)^{1/2}$. Because the traction and the fault slip velocity vectors are collinear, the value of the residual stress is defined according to the direction of motion. Equation (8) is practically identical to the formulation of Bizzarri and Das (2012; their equation 4), as it is discussed in detail in Appendix B.

Equation (8) is valid not only for the SW law but also can be easily generalized to various fault governing models, such as the rate- and state-dependent friction laws (in such a case $\|\mathbf{T}_{\mathrm{res}}(\xi)\| = \tau_f^{\mathrm{eq}}$, following Bizzarri and Cocco, 2003). I remark here that the minus sign appearing in front of the integral in equation (2.18) of Achenbach (1972) is cancelled because of our definition of the discontinuity of the particle velocity fields, that is, of the fault slip velocity $v_i = V_i^+ - V_i^-$, in which V_i^+ and V_i^- are the components of the particle velocity on the two half-spaces of the oriented fault surface (see also fig. 3 of Bizzarri and Spudich, 2008); and $v_2 = 0$, because the material interpenetration and the opening of the fault are not allowed. The numerical counterpart of (8) is

$$\tilde{F}^{(m)} = (\Delta x)^2 \sum_{(i,k)} \sum_{\in \tilde{\Pi}^{(m)}} \left(\tilde{T}_1^{(m)}(i,k) - \tau_f \frac{\tilde{v}_1^{(m)}(i,k)}{\tilde{v}^{(m)}(i,k)} \right) \tilde{v}_1^{(m)}(i,k) + \left(\tilde{T}_3^{(m)}(i,k) - \tau_f \frac{\tilde{v}_3^{(m)}(i,k)}{\tilde{v}^{(m)}(i,k)} \right) \tilde{v}_3^{(m)}(i,k), \quad (9)$$

in which the summation is done for the doublets (i,k), which at each time level m define the region $\tilde{\Pi}^{(m)}$ surrounding the crack tip. A schematic representation of the integration domain is reported in Figure 1. The definition of the crack tip, $\Gamma(t) = \{(x_1, x_3) | v(x_1, x_3, t) \geq v_l \text{ for the first time}\}$, can be rewritten in discrete terms as $\tilde{\Gamma}^{(m)} = \{(i,k) | \tilde{t}_r(i,k) = m\}$, in which m denotes the time level ($\tilde{t}^{(m)} = m\Delta t$, with Δt being the time step). In the 2D singular crack of Achenbach (1972; see fig. 2) the region $\Pi(t)$ is defined by the interval $[x_r(t) - \varepsilon, x_r(t) + \varepsilon]$, in which $x_r(t)$ is the instantaneous location of the rupture tip at time t and ε is an arbitrarily small positive real number. In our nonsingular fault model, the region $\Pi(t)$ is a zone surrounding the rupture tip and is sufficiently large to account for the dissipative processes occurring during the failure, that is, the length of the cohesive zone $X_b(t)$. This is the substantial difference between the treatment of Achenbach (1972), which is valid only for singular cracks, and our generalization to constitutive models with cohesive zone.

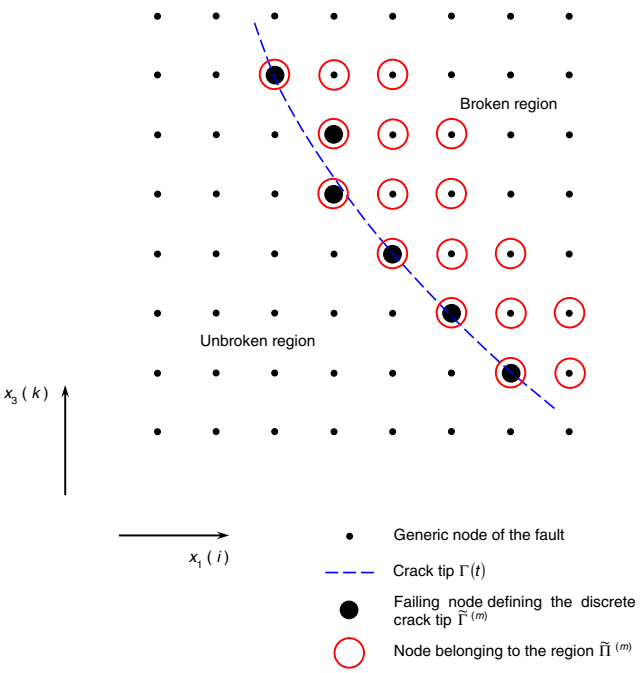

Figure 1. Diagrammatic representation of the region $\tilde{\Pi}^{(m)}$ used to compute the energy rate F in equation (8). The crack tip at time t, $\Gamma(t)$ (dashed line), is defined by the fault nodes having a slip velocity exceeding the threshold value v_l. Large black circles formally define $\tilde{\Gamma}^{(m)}$. The large open circles denote the nodes that define the region $\tilde{\Pi}^{(m)}$. For simplicity I represent $\tilde{\Pi}^{(m)}$ only with 3 points at each depth; this is only a simplified sketch, in that the region $\Pi(t)$ represents the length of the cohesive zone $X_b(t)$, which is mapped by a large number of points (due to the very fine discretization I employ). The color version of this figure is available only in the electronic edition.

To define the region $\tilde{\Pi}^{(m)}$, in our 3D case I consider all the nodes belonging to the process zone; that is, up to a distance from the rupture tip where the traction has already reached the residual level τ_f; these nodes are denoted by large open circles in Figure 1. To illustrate this, let the doublet (i^*, k^*) denote a generic fault node that fails. Let also $i \geq i^*$ define the broken region, for the given depth $(k^* - 1)\Delta x$ (see Fig. 1). Because the breakdown process is not abrupt (contrarily to Achenbach [1972], but it is controlled by the constitutive relation that incorporates the cohesive forces), for the given depth $(k^* - 1)\Delta x$ it is not true the fault traction exactly equals τ_f for $i > i^*$. In particular, as a result of the assumed spatiotemporal resolution of the cohesive zone, I now have $\tilde{\tau}^{(m)}(i^* + 1, k^*) > \tau_f$.

Results for Nonspontaneous Ruptures

In this section, I consider synthetic earthquakes that propagate over the fault in a nonspontaneous fashion, that is, with a prescribed and constant rupture speed v_r. The adopted parameters are listed in Table 1. In these numerical simulations, the ruptures are nonsingular, in that the stress drop is accomplished over a characteristic, and finite, time $t_0 = 0.1$ s; namely, this is a time-weakening friction law (see equation 23 in Bizzarri, 2011), which can be regarded as the counterpart of the SW law in the time domain. The results for four selected configurations are reported in Figure 2, from which I can see that F is always positive and increasing, in agreement with the findings of Bizzarri and Das (2012). Moreover, it emerges that after an initial stage the rate of increase of F becomes nearly constant, and this rate is proportional to the rupture speed. To interpret this result, I consider, in the interest of simplicity, a circular 3D rupture that propagates on a homogeneous fault with a constant speed. The rate of the variation of the broken region can be approximated as $\dot{\Sigma}(t) \cong 2\pi v_r^2 t$, so that from equation (5) we can write $F(t) \cong 2\pi v_r^2 E_G t$. Therefore, for this specific configuration, I have: $\dot{F}(t) \cong 2\pi v_r^2 E_G$. If I also assume that E_G is uniform over the whole fault, I finally have that $\dot{F}(t)$ is constant and proportional to v_r^2. In our case this relation cannot be used literally, in that the shape of the rupture front is not perfectly circular.

It is interesting to note that one of the models (dashed line in Fig. 2) propagates with a constant velocity that is within the forbidden zone. Although this seems to be in contrast to the theory, we must recall that the negative energy flux is predicted for 2D steady-state singular cracks. I repeat here that our ruptures are not singular, and therefore F is positive (and nondecreasing) also near the boundaries and within the forbidden zone. I finally emphasize that even in pure mode II ruptures, if they are nonsingular, one can obtain the rupture propagation at a constant speed within the forbidden zone.

Table 1
Parameters Adopted in the Present Paper

Parameter	Value
Medium and discretization parameters	
Lamé constants, $\lambda = G$	35.9 GPa
S-wave velocity, v_S	3.464 km/s
Rayleigh velocity, v_R	3.184 km/s
P-wave velocity, v_P	6 km/s
Eshelby velocity, $v_E = \sqrt{2}v_S$	4.899 km/s
Fault length, L^f	16 km
Fault width, W^f	12 km
Spatial grid size, Δx	5 m
Final time, t_{end}	3.12 s
Time step, Δt	1.2×10^{-4} s
Coordinates of the hypocenter, $H \equiv (x_1^H, x_3^H)$	(8,7) km
Fault constitutive parameters	
Magnitude of the effective normal stress, σ_n^{eff}	120 MPa
Magnitude of the initial shear stress (prestress), τ_0	73.8 MPa
Static friction coefficient, μ_u	0.677 ($\leftrightarrow \tau_u = 81.24$ MPa)
Dynamic friction coefficient, μ_f	0.46 ($\leftrightarrow \tau_f = 55.20$ MPa)
Resulting strength parameter, S	0.4
Characteristic slip-weakening distance, d_0	0.4 m

Spontaneous Modeling

I now consider a fully spontaneous rupture, where v_r is not previously assigned (as in the Results for Nonspontaneous Ruptures section), but it changes during the propagation process and is a part of the solution of the elastodynamic problem. The fault obeys a linear SW law (see equation 25 in Bizzarri, 2011) and the parameters are again those of Bizzarri and Das (2012); see Table 1. By definition, the ruptures are not singular. I do not prescribe any arrest of the rupture, because the fault properties are homogeneous and no healing mechanisms are incorporated into the fault governing law. The synthetic event represents an earthquake having a seismic

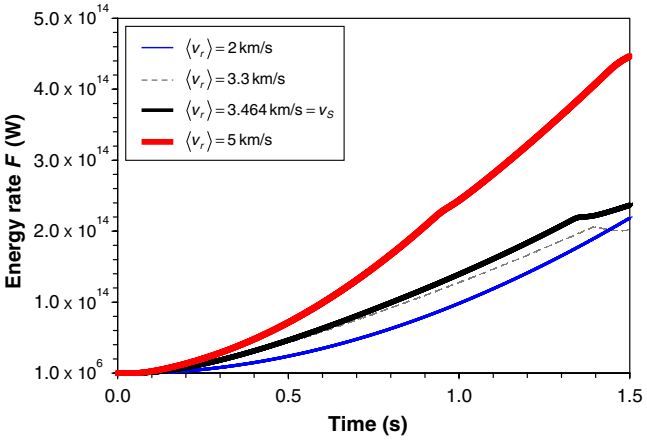

Figure 2. Energy flux $F(t)$ for ruptures with prescribed and constant velocity over the whole fault surface (i.e., nonspontaneous rupture models, but still with cohesive force). The dashed line represents a case in which rupture speed is within the forbidden zone. The color version of this figure is available only in the electronic edition.

moment M_0 2.18×10^{19} N·m (M_w 6.83). Just to give a rough idea this synthetic event is slightly smaller than the 1995 Hyogo-ken Nanbu (Kobe, Japan) earthquake (Wald, 1996).

The time evolution of F is reported in Figure 3a; the dots indicate F as computed from the rate of variation of U_G (i.e., computed from equation 5), while the continuous lines denote F as computed from the integration of traction and slip velocity (i.e., computed from equation 8). A first outcome emerging from Figure 3a is that the two different and independent calculations give the same result. This indicates that equation (5)—which has been derived theoretically in the case of quasistatic (Cherepanov, 1967; Rice, 1968) or steady-state ruptures (Ida, 1972), as discussed in the Introduction—is a sufficiently good approximation also in the case of variable rupture speeds, for which seismic-wave radiation is expected (Madariaga, 1983).

I can also see that the value of F resulting from equation (8) is basically due to the 1-components of traction and slip velocity; the 3-components contribute only a little in the total F. The peak in F at $t = 2.049$ s and its further decrease is attributed to the fact that at that time the rupture front hits the fault boundary $x_1 = 0$, as clearly depicted in Figure 3b, where I plot the spatial distribution of the rupture times. After that instant the definition of the rupture tip becomes problematic, in that part of it begins to be absorbed by the fault boundary, so that a diminishing (and finally null) part of it remains defined. I can therefore disregard the behavior of F after $t = 2.049$ s.

Another interesting time is $t = 1.71$ s, the time when the rupture tip first hits the bottom of the fault, as also reported in Figure 3b. At this time it is possible to clearly see variation of the rate of increase of F (see Fig. 3a). In particular, we observe that $\dot{F}$ decreases after $t = 1.71$ s; this is also due to the fact that after this instant the deeper part of the rupture tip is not properly defined, as observed above, and only its shallow part remains. I also remark a significant increase in $\dot{F}$ after $t = 0.7998$ s; this represents the time when the rupture begins to propagate in a supersonic fashion (see Fig. 3b).

Overall, I emphasize that F is always increasing as in the nonspontaneous simulations (see the Results for Nonspontaneous Ruptures section). In Figure 4, the evolution of F as a function of v_r is reported (note that in this case we plot the energy flux resulting from equation 8, not just the contribution of the nodes aligned in the mode II direction or in the mode III direction, as done in fig. 6 of Bizzarri and Das [2012]). From Figure 4 it emerges that F is positive over the whole range of rupture speeds (from 0 to v_P) and does not exhibit relevant variations in its rate, contrary to what happens in 2D, in which the increase of F tends to vanish just below the beginning of the forbidden zone (i.e., when v_r approaches v_R). As long as the rupture propagates in a sustained supershear way, F increases more rapidly; this can be interpreted in two ways. First, from equation (5) we note that, since E_G is constant in time and homogeneous in space, the energy flux into the process zone is directly proportional to the rate of increase of the ruptured area; as the rupture becomes supershear, after $t = 0.7998$ s (see Fig. 3b), the fault surface is consumed faster. Another interpretation comes from equation (8). Once the rupture becomes supershear, the slip velocity tends to increase, due to the contraction of the cohesive zone (see appendix A of Bizzarri *et al.*, 2001, and fig. 4d of Bizzarri and Das, 2012; we can also numerically verify that the peaks in slip velocity globally increase), and this makes the integrand in equation (8) larger.

Finally, I remark that even in the mode II direction the cohesive zone does not vanish, as the Rayleigh speed is approached (Bizzarri and Das, 2012), and this removes the singularity in the integration domain which would potentially appear in a 2D, pure mode II rupture.

The results discussed above are also preserved in the case of a subshear event. I consider a case in which the parameters are exactly the same as in the supershear event, except for the initial shear stress, which is now 63.88 MPa instead of 73.8 MPa. This value gives a higher value of the strength parameter S (Das and Aki, 1977), which is now 2 instead of 0.4, but the breakdown stress drop is the same in both models, so E_G is also the same. In this case it gives M_0 9.26×10^{18} N·m or equivalently M_w 6.58, which is slightly greater than the magnitude of the 1979 Imperial Valley, California, earthquake (Hartzell and Heaton, 1983).

A first outcome of Figure 5 is that the value of the energy flux is significantly reduced with respect to the supershear event. This is not surprising, considering that for a less unstable fault we expect to have small slip velocities compared to a very unstable fault. Moreover, also in this case the contribution due to the 3-component (i.e., the along-depth component) is even less significant in the computation of the total F. This also is not surprising, because the maximum rake variation (which in turn corresponds to a deviation of $T_3 v_3$ from $\tau_f v_3^2 / v$) is maximum in correspondence to the supershear transition, as already discussed in Bizzarri and Das (2012).

Discussion and Concluding Remarks

In this paper, I generalize the calculation of the energy flux F at the tip of a propagating rupture, originally formulated by Achenbach (1972) in the case of 2D singular cracks (for which the stress release is abrupt and is accomplished in an arbitrarily small process zone). Here I consider an extended fault, with 3D geometry, for which mode II and mode III are mixed together and the rake variation is allowed. In our case the stress release is not abrupt, as in singular crack models, but it occurs over a characteristic time—the breakdown time T_b—which is controlled by the characteristic length scale of the assumed fault governing law. Correspondingly, the process zone has a finite dimension in space—the breakdown distance X_b. The general expression of the time evolution of the energy flux is given by equation (8), which is valid for various fault governing models in which the residual level of friction is well defined.

By considering both nonspontaneous (i.e., with prior assigned rupture speed v_r) and spontaneous synthetic

earthquakes obeying a fault governing law with cohesive zone, I show that F is always positive and increasing, and it does not have any relevant variation in its rate. This result is not obvious because, in 2D dynamic and spontaneous ruptures obeying the linear SW law, the energy flux rate tends to vanish or even decrease when the forbidden zone is approached. The positiveness and the increasing behavior of F confirms previous findings of Bizzarri and Das (2012), who demonstrated that along the direction of pure mode II, and that of pure mode III, F is always increasing with

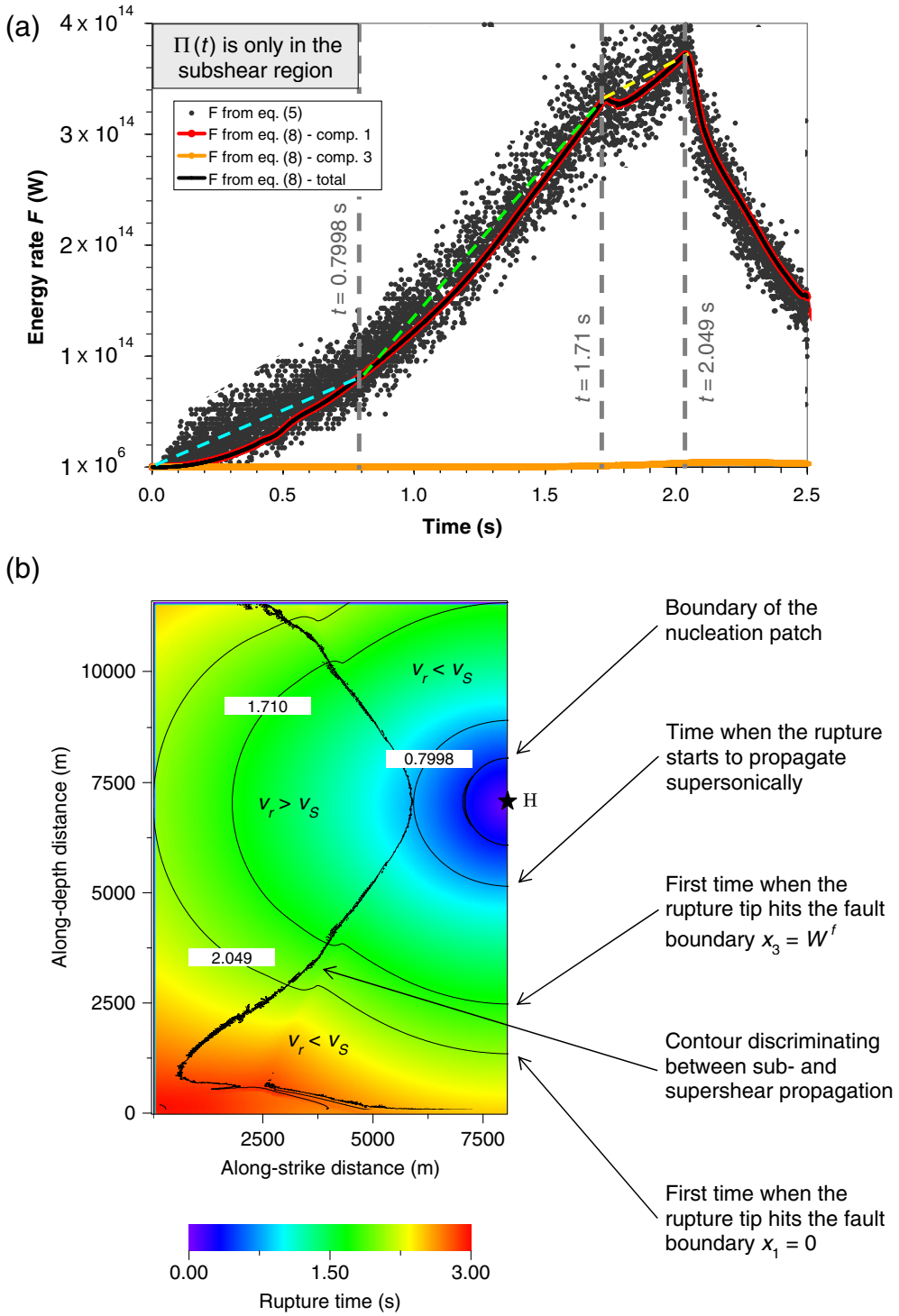

Figure 3. (a) Time evolution of $F(t)$ for a spontaneous rupture, as computed from equations (5) and (8) (dots and continuous lines, respectively). Components 1 and 3 refer to the component of traction and slip velocity aligned along the strike and the depth directions, respectively, for the geometry assumed here. (b) Spatial distribution of the rupture times, with some relevant times indicated. The color version of this figure is available only in the electronic edition.

time. Moreover, in the case of supershear ruptures, the fact that F is positive over the whole range of v_r (see Fig. 4) is in contrast with the theoretical results pertaining to 2D steady-state singular cracks (e.g., Broberg, 1999).

Indeed, the mechanics of a curved 3D rupture front cannot be adequately described by using the results from 2D plane front, except when the cohesive zone is small compared to the radius of curvature of the 3D rupture tip. This can occur when (1) the cohesive zone is extremely small at the supershear transition and (2) the supershear transition occurs in a very late stage of the rupture (i.e., very far from the hypocenter), so that curvature of the rupture front is very small. Both these situations pose relevant problems of numerical resolutions (I recall that, due to its contraction [e.g., Andrews, 1976; Bizzarri and Das, 2012], it is very difficult to have sufficiently good resolution of the cohesive zone at huge distances from the imposed hypocenter).

The fact that the energy flux is also positive in the so-called forbidden zone can be theoretically illustrated by considering equation (3.2.64) of Dmowska and Rice (1986; see also Kostrov and Nikitin, 1970):

$$E_G = \frac{1}{2G}[(1-\nu)(g^{(\mathrm{II})}K^{(\mathrm{I})2} + g^{(\mathrm{I})}K^{(\mathrm{II})2}) + g^{(\mathrm{III})}K^{(\mathrm{III})2}], \tag{10}$$

in which G is the rigidity of the medium, ν is the Poisson ratio, and $K^{(\mathrm{I})}$, $K^{(\mathrm{II})}$, and $K^{(\mathrm{III})}$ are the stress intensity factors for the three linearly independent basic modes of rupture in fracture mechanics (I, II, and III, respectively). K physically expresses the state of the stress near the tip of a crack due to a remote loading. The functions g, defined in equation (3.2.63) of Dmowska and Rice (1986), depend explicitly on v_r, increase monotonically with v_r, and become unbounded for the limiting speeds v_R for modes I and II and v_S for mode III (they are also related to the inverse of the functions F in equation 11 in Bizzarri, 2012). Indeed, equation (10) is of completely general validity for crack motion at steady or unsteady sub-Rayleigh speed (or subshear speed in the case of a pure mode III crack) propagating in a linear and isotropic elastic medium. Now, from equation (5) I simply have (for the linear SW law)

$$F(t) = \frac{\dot{\Sigma}(t)}{2G}[(1-\nu)(g^{(\mathrm{II})}K^{(\mathrm{I})2} + g^{(\mathrm{I})}K^{(\mathrm{II})2}) + g^{(\mathrm{III})}K^{(\mathrm{III})2}], \tag{11}$$

from which it is possible to see that the energy flux is expressed by a mixture of functions g defined in the two overlapping intervals of v_r $[0, v_R]$ and $[0, v_S]$.

Another interesting outcome of the present study is that F is somehow proportional to v_r; from Figure 2, in which F for nonspontaneous and nonsingular ruptures is reported, it can be seen that fast earthquakes tend to have a higher energy flux at the rupture tip compared to slower events. The relation between the fracture energy density, E_G, and the rupture speed, has been already discussed elsewhere (Bizzarri, 2010). Here I found that, again in contrast to steady-state solutions, F increases as v_r increases. Remarkably, there are no decreases in the energy flux as the rupture speed approaches the limiting speed of v_P, nor when it approaches the forbidden zone (see Fig. 4).

Remarkably, the results presented in this study show that equation (5)—which follows from equation (3), which in turn has been theoretically derived for quasistatic (Cherepanov, 1967; Rice, 1968) or steady-state ruptures (Ida, 1972)—also is a sufficiently good approximation in the case of nonsteady ruptures (i.e., with variable rupture speeds), for which seismic-wave radiation is expected (Madariaga, 1983). This is apparent from the different computation presented in Figure 3a.

Finally, I found here that the magnitude of the energy rate at the rupture tip is basically controlled by its component aligned as the initial shear stress (see Figs. 3a and B1). In our case of a strike-slip faulting mechanism F is essentially due

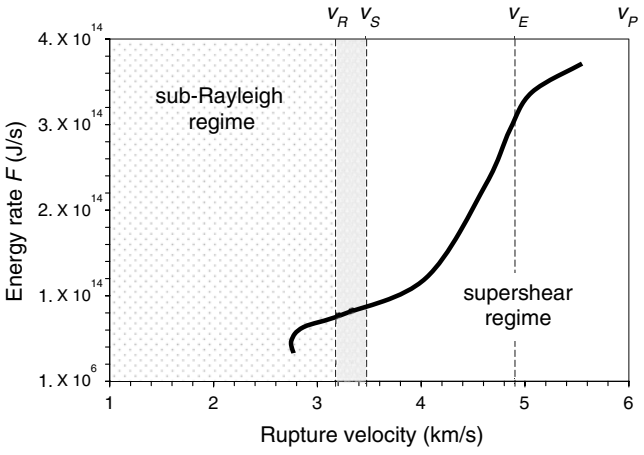

Figure 4. Energy flux as a function of rupture speeds in the case of supershear rupture of Figure 3. Relevant rupture speeds are indicated, as well as the forbidden zone.

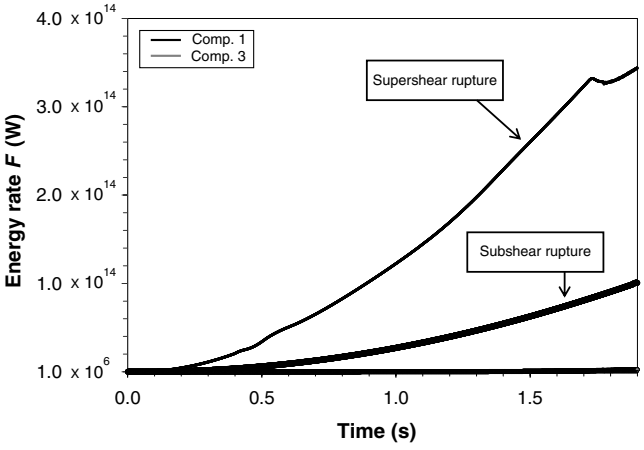

Figure 5. Time evolution of $F(t)$ in the case of subshear rupture (thick lines). The results pertaining to the supershear rupture of Figure 3 are also reported as thin lines for comparison. In both cases black color refers to the 1-component (i.e., the strike-slip component), while gray color refers to the 3-component (i.e., the along-depth component) of the integrand function of equation (8).

to the 1-components of traction and slip velocity; from Figure 3a we see that $F^{(II)}(t)$ is definitively paramount with respect to $F^{(III)}(t)$. This clearly demonstrates that the rake rotation does not play a substantial role in the earthquake energy balance.

Data and Resources

All data sources were taken from published works listed in the References.

Acknowledgments

The author thanks S. Das for valuable discussions that motivated this study and R. Madariaga for stimulating comments. He also acknowledges Associate Editor A. McGarr and two anonymous referees who provided detailed comments that help in clarifying some points in the paper.

References

Achenbach, J. D. (1972). Dynamic effects in brittle fracture, in *Mechanics Today 1*, S. Nemat-Nasser (Editor), Pergamon Press, New York, 1–57.

Andrews, D. J. (1976). Rupture velocity of plane strain shear cracks, *J. Geophys. Res.* **81,** 5679–5687.

Atkinson, C., and J. D. Eshelby (1968). The flow of energy into the tip of a moving crack, *Int. J. Fract. Mech.* **4,** no. 1, 3–8.

Bizzarri, A. (2009). Can flash heating of asperity contacts prevent melting?, *Geophys. Res. Lett.* **36,** L11304, doi: 10.1029/2009GL037335.

Bizzarri, A. (2010). On the relations between fracture energy and physical observables in dynamic earthquake models, *J. Geophys. Res.* **115,** no. B10307, doi: 10.1029/2009JB007027.

Bizzarri, A. (2011). On the deterministic description of earthquakes, *Rev. Geophys.* **49,** RG3002, doi: 10.1029/2011RG000356.

Bizzarri, A. (2012). Analytical representation of the fault slip velocity from spontaneous dynamic earthquake models, *J. Geophys. Res.* **117,** no. B06309, doi: 10.1029/2011JB009097.

Bizzarri, A., and M. Cocco (2003). Slip-weakening behavior during the propagation of dynamic ruptures obeying rate- and state-dependent friction laws, *J. Geophys. Res.* **108,** no. B8, 2373, doi: 10.1029/2002JB002198.

Bizzarri, A., and M. Cocco (2005). 3D dynamic simulations of spontaneous rupture propagation governed by different constitutive laws with rake rotation allowed, *Ann. Geophys.* **48,** no. 2, 279–299.

Bizzarri, A., and S. Das (2012). Mechanics of 3D shear cracks between Rayleigh and shear wave rupture speeds, *Earth Planet. Sci. Lett.* **357–358,** 397–404, doi: 10.1016/j.epsl.2012.09.053.

Bizzarri, A., and P. Spudich (2008). Effects of supershear rupture speed on the high-frequency content of S waves investigated using spontaneous dynamic rupture models and isochrone theory, *J. Geophys. Res.* **113,** no. B05304, doi: 10.1029/2007JB005146.

Bizzarri, A., M. Cocco, D. J. Andrews, and E. Boschi (2001). Solving the dynamic rupture problem with different numerical approaches and constitutive laws, *Geophys. J. Int.* **144,** 656–678.

Broberg, K. B. (1989). The near-tip field at high crack velocities, *Int. J. Fract.* **39,** 1–13.

Broberg, K. B. (1999). *Cracks and Fracture*, Academic Press, New York, 752 pp.

Cherepanov, G. P. (1967). The propagation of cracks in a continuous medium, *J. Appl. Math. Mech.* **31,** no. 3, 503–512.

Curran, D. A., D. A. Shockey, and S. Winkler (1970). Crack propagation at supersonic velocities, II, Theoretical model, *Int. J. Fract. Mech.* **6,** 271–278.

Das, S., and K. Aki (1977). A numerical study of two-dimensional spontaneous rupture propagation, *Geophys. J. Roy. Astron. Soc.* **50,** 643–668.

Dmowska, R., and J. R. Rice (1986). Fracture theory and its seismological applications, in *Continuum Theories in Solid Earth Physics, in Physics and Evolution of the Earth's Interior*, No. 3 R. Teisseyre (Editor), Elsevier and Polish Scientific Publishers, 187–255.

Favreau, P., and R. J. Archuleta (2003). Direct seismic energy modeling and application to the 1979 Imperial Valley earthquake, *Geophys. Res. Lett.* **30,** no. 5, 1198, doi: 10.1029/2002GL015968.

Freund, L. B. (1972). Energy flux into the tip of an extending crack in an elastic solid, *J. Elasticity* **2,** 341–350.

Freund, L. B. (1979). Mechanics of dynamic shear crack–propagation, *J. Geophys. Res.* **84,** no. B5, 2199–2209.

Freund, L. B. (1990). *Dynamic Fracture Mechanics*, Cambridge University Press, Cambridge, England.

Griffith, A. A. (1920). The phenomenon of rupture and flow in solids, *Phil. Trans. Roy. Soc. Lond. A* **221,** 163–198.

Hartzell, S. H., and T. H. Heaton (1983). Inversion of strong ground motion and teleseismic waveform data for the fault rupture history of the 1979 Imperial Valley, California, earthquake, *Bull. Seismol. Soc. Am.* **73,** 1553–1583.

Ida, Y. (1972). Cohesive force across the tip of a longitudinal-shear crack and Griffith's specific surface energy, *J. Geophys. Res.* **77,** no. 20, 3796–3805.

Kostrov, B. V., and L. V. Nikitin (1970). Some general problems of mechanics of brittle fracture, *Arch. Mech. Stos.* **22,** 749–775, (in Russian).

Madariaga, R. (1983). High frequency radiation from dynamic earthquake fault models, *Ann. Geophys.* **1,** 17–23.

Madariaga, R. (2012). The birth of forward models: From Coulomb criterion to cohesive force laws, in *The Mechanics of Faulting: From Laboratory to Real Earthquakes*, A. Bizzarri and S. H. Bhat (Editors), Research Signpost, India, http://www.ressign.com/UserArticleDetails.aspx?arid=11588#; http://trnres.com/emags/bizzarri/bizzarriebook.html (last accessed May 2013), 125–152.

Rice, J. R. (1968). A path independent integral and the approximate analysis of strain concentration by notches and cracks, *J. Appl. Mech.* **35,** 379–386.

Rivera, L., and H. Kanamori (2005). Representation of the radiated energy in earthquakes, *Geophys. J. Int.* **162,** 148–155, doi: 10.1111/j.1365-246X.2005.02648.x.

Samudrala, O., Y. Huang, and A. J. Rosakis (2002). Subsonic and intersonic shear rupture of weak planes with a velocity weakening cohesive zone, *J. Geophys. Res.* **107,** no. B8, doi: 10.1029/2001JB000460.

Wald, D. J. (1996). Slip history of the 1995 Kobe, Japan, earthquake determined from strong motion, teleseismic, and geodetic data, *J. Phys. Earth* **44,** no. 5, 489–503.

Winkler, S., D. A. Shockey, and D. A. Curran (1970). Crack propagation at supersonic velocities I, *Int. J. Fract. Mech.* **6,** 151–158.

Appendix A

Link between Equations (3) and (6)

In this section, I will demonstrate that, in the case of 2D rupture problem and by assuming the linear slip-weakening (SW) friction law, equation (3) can be obtained from equation (6). To this goal, let me rewrite equation (6) in this special case:

$$F(t) = \int_{\pi(t)} f(x_1, t)\mathrm{d}x_1, \tag{A1}$$

in which $\pi(t)$ is the counterpart in 2D of the domain of integration $\Pi(t)$ in 3D (see also Fig. 1) and

$$f(x_1,t) \equiv (\tau(x_1,t) - \tau_f)v(x_1,t). \tag{A2}$$

In the case of the linear SW law, the domain of integration $\pi(t)$ can be made explicit as it follows: $x_1 \in [0, \sigma(t)]$, in which $\sigma(t)$ is the fractured area at time t (namely, it represents the location of the rupture front at time t) and for which we have considered only one half of a bilateral rupture starting at $t = 0$ from the point $x_1 = 0$. ($\sigma(t)$ formally is the counterpart in 2D of the region denoted by the symbol $\Sigma(t)$ in 3D; see equation 4). Equation (A1) then becomes

$$F(t) = \int_0^{\sigma(t)} f(x_1,t)\mathrm{d}x_1. \tag{A3}$$

Let T be an arbitrary time greater than the actual time t, so that $\sigma(T) > \sigma(t)$. In the case of linear SW law, one has

$$f(x_1,t) = 0, \quad \forall\ x_1 > \sigma(t), \tag{A4}$$

simply because $v = 0$ in the unbroken part of the fault. Therefore I can rewrite equation (A3) as

$$F(t) = \int_0^{\sigma(T)} f(x_1,t)\mathrm{d}x_1. \tag{A5}$$

After integrating $F(t)$ of equation (A5) over the time t, between 0 and T, I have

$$\begin{aligned}\int_0^T F(t)\mathrm{d}t &= \int_0^T \int_0^{\sigma(T)} f(x_1,t)\mathrm{d}x_1\,\mathrm{d}t \\ &= \int_0^{\sigma(T)} \int_0^T f(x_1,t)\mathrm{d}t\,\mathrm{d}x_1 \\ &= \int_0^{\sigma(T)} E_G(x_1)\mathrm{d}x_1 \\ &= U_G(T),\end{aligned} \tag{A6}$$

in which I have changed the order of integration in the second line and have considered the definitions of the fracture energy density (see equation 1) and of the total fracture energy (see equation 4) in the third and fourth lines, respectively. By differentiating with respect to the time T in both the members of equation (A6), I finally have

$$F(t)|_{t=T} - F(t)|_{t=0} = \frac{\mathrm{d}}{\mathrm{d}T} U_G(T), \tag{A7}$$

which simply reads:

$$F(T) = \dot{U}_G, \tag{A8}$$

because $F(0) = 0$ (recall that $f(x_1, 0) = 0$ for the SW law, because $v(x_1, 0) = 0$). Whereas T is arbitrary, I can replace T with t in equation (A8), so that (A8) is exactly the same as equation (3).

I emphasize that the above demonstration holds exactly only in the case of linear SW law. In more elaborate constitutive models (such as the rate- and state-dependent friction laws), the condition (A4) does not hold, in that the fault slip velocity is (although small) nonnull also in the unbroken part of the fault, so that we cannot replace (A3) with (A5). In turn, this prevents the change in the order of integration performed in equation (A6).

Appendix B

Comparison of Two Formulations to Compute the Energy Flux F

When no rake rotation is allowed during the rupture processes the traction is always aligned with the initial shear stress and the slip-weakening (SW) governing law can be simply specified, at each time t, through the Euclidean norm of the shear stress vectors ($\tau_0 = \|\mathbf{T}_0\|$, $\tau_u = \|\mathbf{T}_u\|$ and $\tau_f = \|\mathbf{T}_{\mathrm{res}}\|$). The situation is more complicated when rake rotation is allowed, as in the simulations presented and discussed in the present paper (see also Bizzarri and Cocco, 2005).

Although traction and fault slip velocity vectors are collinear, at each time t we can express the difference between the actual traction $\mathbf{T}$ and the residual level $\mathbf{T}_{\mathrm{res}}$ as it follows $(T - \tau_f)\frac{v_1}{v}$ along x_1 and $(T - \tau_f)\frac{v_3}{v}$ along x_3 (with $T = \|\mathbf{T}\|$ and $v = \|\mathbf{v}\|$). By definition, we also have $T\frac{v_1}{v} = T_1$ and $T\frac{v_3}{v} = T_3$. Therefore, from equation (6) we have

$$F(t) = \iint_{\Pi(t)} \left[\left(T_1 - \tau_f \frac{v_1}{v} \right) v_1 + \left(T_3 - \tau_f \frac{v_3}{v} \right) v_3 \right] \mathrm{d}x_1 \mathrm{d}x_3, \tag{B1}$$

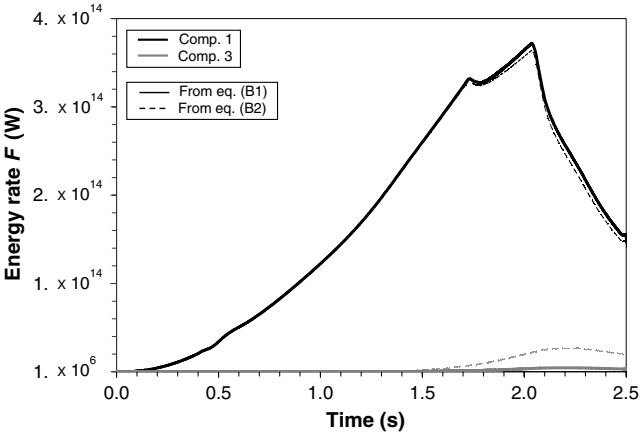

Figure B1. Comparison between the computation of $F(t)$ from two different methods; equation (B1) (full lines) assumes that the residual stress is defined from the collinearity of slip velocity and traction vectors, equation (B2) (dashed lines) assumes that it is collinear with the initial shear stress vector (see Appendix B for further details).

which is equation (8) of the main paper, where we have dropped the explicit dependence on the spatial coordinates and on time in the integrand.

Bizzarri and Das (2012; their equation 4) use a slightly different equation, which assumes that $\mathbf{T}_{\text{res}}$ is always collinear to $\mathbf{T}_0$ (for the adopted faulting mechanism, we have $\mathbf{T}_{\text{res}} = (\tau_f, 0)$). In such a case, we have

$$F(t) = \iint_{\Pi(t)} [(T_1 - \tau_f) v_1 + T_3 v_3] \mathrm{d}x_1 \mathrm{d}x_3. \qquad \text{(B2)}$$

From the comparison of equations (B1) and (B2), it is apparent that the integrand functions are $T_1 v_1 + T_3 v_3 - \tau_f v = Tv - \tau_f v$ in the first case and $T_1 v_1 + T_3 v_3 - \tau_f v_1 = Tv - \tau_f v_1$ in the second one.

In Figure B1 we compare the results from the two formulations (B1) and (B2). The parameters are the same as in Figure 3 (see Table 1); we have deliberately chosen the supershear simulation because it is known that subshear models should have much smaller rake rotations. It is clear that variations are negligible; they begin to become appreciable only after $t = 1.71$ s, which corresponds to the time when the rupture tip first hits the bottom of the fault (see Fig. 3b and the Results for Nonspontaneous Ruptures section of the main text). Before this point the two time evolutions of F are identical, for both the 1-component and 3-component. Because the 3-component is practically negligible in the total estimate of F, we can conclude that the two methods are equally good estimates of the energy flux.

Istituto Nazionale di Geofisica e Vulcanologia
Sezione di Bologna
Via Donato Creti, 12
40128 Bologna, Italy
bizzarri@bo.ingv.it

Manuscript received 14 November 2012